

# CFD DESIGN OF PROTECTIVE WALLS AGAINST THE EFFECTS OF VAPOR CLOUD FAST DEFLAGRATION OF HYDROGEN

Vyazmina, E.<sup>1</sup>, Jallais, S.<sup>1</sup>, Beccantini, A.<sup>2</sup> and Trelat, S.<sup>3</sup>

<sup>1</sup> Centre de Recherche Paris-Saclay, AIR LIQUIDE Research & Development, 1, chemin de la Porte des Loges, Les Loges-en-Josas - BP 126, 78354, Jouy-en-Josas, France,

Elena.Vyazmina@airliquide.com Simon.Jallais@airliquide.com

<sup>2</sup> Department 2, CEA Saclay DM2S/STMF/LATF, Street, (P.O.Box if any), City, Post code, France, Alberto.Beccantini@cea.fr

<sup>3</sup> Department 3, IRSN, Street, (P.O.Box if any), City, Post code, France, Sophie.Trelat@irsn.fr

## ABSTRACT

Protective walls are a well-known and efficient way to mitigate overpressure effects of accidental explosions (detonation or deflagration). For detonation there are multiple published studies, whereas for deflagration no well-adapted and rigorous method has been reported in the literature. This article describes the validation of a new modeling approach for fast deflagrations of H<sub>2</sub>. This approach includes two steps. At the first step, the combustion phase of vapor cloud explosion (VCE) involving a fast deflagration is substituted by equivalent vessel burst problem. The purpose of this step is to avoid the reactive flow computations. At the second step, CFD is used for computations of pressure propagation from the equivalent (non reactive) vessel burst problem. After verifying the equivalence of the fast deflagration and the vessel burst problem at the first step, the capability of two CFD codes such as FLACS and Europlexus are examined for modeling of the vessel burst problem (with and without barriers). Finally, the efficiency of finite and infinite barriers used for mitigation of the shock is investigated.

## 1.0 INTRODUCTION

Protective walls are an efficient way to protect people and infrastructures from overpressure effects due to accidental or malicious explosions (detonation or deflagration). For detonations, there are several engineering or CFD-based design rules for barricades design in the literature, such as NOTA recommendations 2009 [1], [2] and [3]. However, in case of a deflagration (the most probable industrial scenario), no adapted rigorous method has been published in the open literature. Due to the complexity of the phenomena associated with the interaction between a wall and the blast waves appearing from fast deflagration, a CFD-based method has been developed. The aim of this method is to reproduce the decay of a fast deflagration generated blast wave in a far field upstream and downstream of the barrier, without modeling the combustion process associated with deflagration. As a first step, a 3D CFD code is validated against accurate 2D and 1D numerical solution in a free field, then with a virtual infinite wall. As a second step, several design rules are discussed on the basis of a sensibility study using the validated CFD method.

## 2.0 DEFLAGRATION “EQUIVALENT” PROBLEM

For the combustion of a gaseous hemisphere we assume that, before the flame reaches the interface between the gaseous fresh mixture and the surrounding air, the problem can be reduced to 1D point-symmetric flow generated by a constant flame speed. If the medium is homogeneous, the flame width is negligible and the flame velocity is constant, and the solution will be self-similar, as pointed out in the works of Sedov [5] and Kuhl [6]. According to [7] and [8], this solution (which can be accurately evaluated and is called hereafter Sedov solution) reproduces the first stage (*i.e.* combustion stage) of a hemispheric Vapor Cloud Explosion (VCE). Once the combustion is over the second stage of a VCE can be assimilated to the temporal decay of Sedov solution and can be used for the validation of a non-reactive Euler solver of CFD codes used for VCE computations.

This paper focuses on the effects of a fast deflagration in the far field (the propagation of the pressure waves). As shown in details in [9], there is no need to model the combustion process since we are able to replace it with an equivalent vessel-burst problem. Summarizing, the pressure in the burst reservoir is taken equal to the maximum pressure  $P$  of the Sedov solution; the combustion temperature is the one of the burnt mixture. The radius of the reservoir is evaluated by imposing that the vessel has the same energy as the real mixture:

$$\frac{2}{3} \pi R_{rb}^3 \frac{\Delta P}{\gamma - 1} = E, \quad (1)$$

where  $E$  is the combustion energy of the mixture [J];  $\Delta P = P - P_{ambient}$  – the overpressure inside the burst reservoir [Pa];  $\gamma$  - specific ratio for air;  $R_{rb}$  – the radius of the “equivalent” burst reservoir [m].

We have shown that in case of fast deflagrations that, the “vessel burst” temporal decay is equivalent to the decay of the Sedov solution (t), see fig. 1. (see [9] for details)

In the current investigation, the following high-pressure and high-temperature reservoir are considered, see table 1. This corresponds to a flame velocity of 270 m/s (0.8 of speed of sound), which is approximately equivalent to the strength index of 7 of the TNO multi-energy method (fast deflagration). Initial conditions for the equivalent reservoir burst problem are presented in Table 1 where  $R_{rb}$  is the radius of the reservoir.

Table 1: Initial conditions for a vessel burst problem.

	Vessel burst ( $R_{rb} < 2.657$ m)	Outside region ( $R_{rb} > 2.657$ m)
Overpressure (barg)	0.8561	0
Temperature (K)	3677	293
Density ( $\text{kg/m}^3$ )	0.1759	1.189
Speed of sound (m/s)	1215	343.1

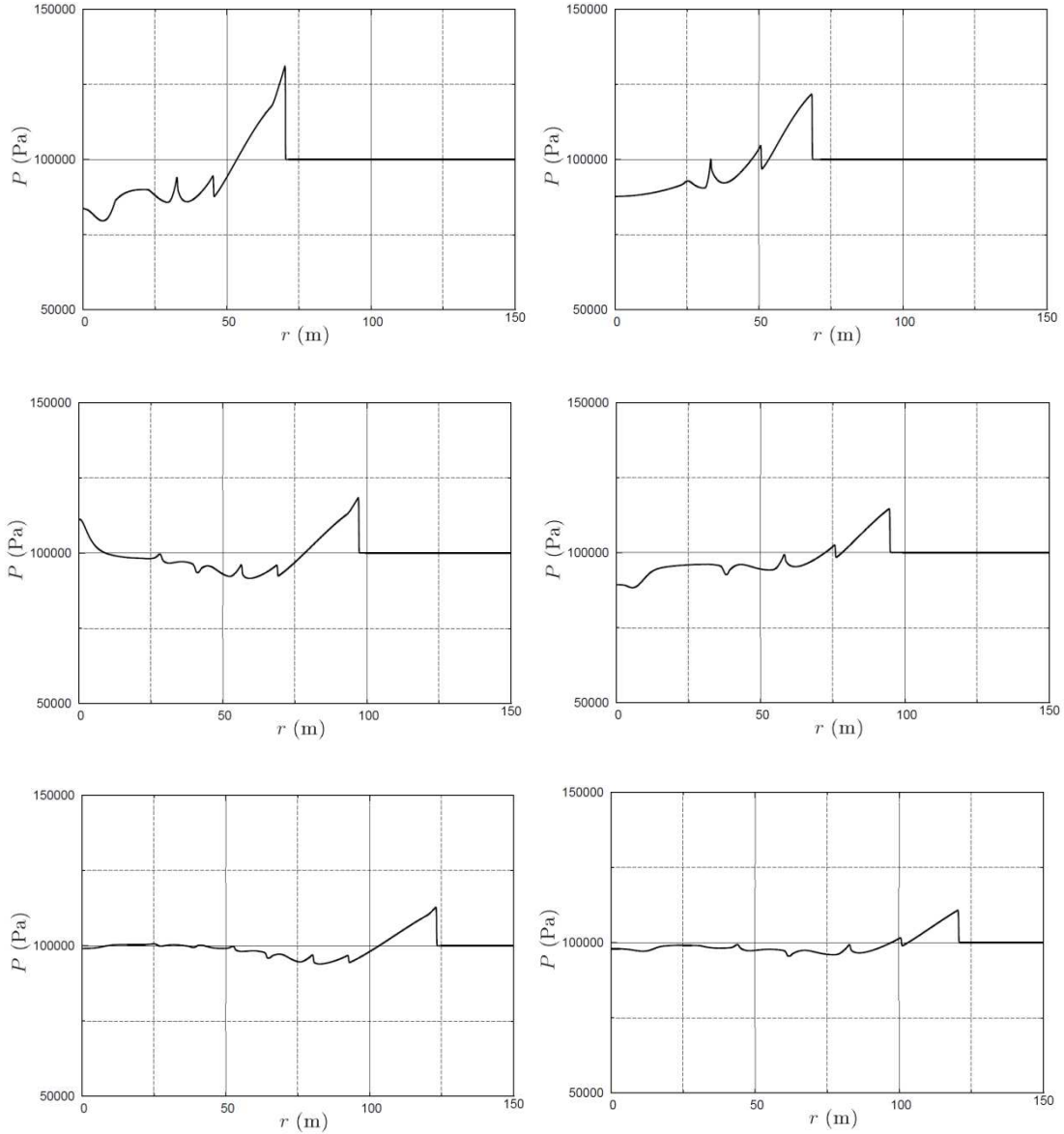


Figure 1. Time decay of the Sedov solution (left) and reservoir problem (right) in the case flame velocity is equal to 0.8 of sound speed at (times  $t=0.1072s$ ,  $t=0.1786s$ ,  $t=0.2501s$ ), adapted from [9].

### 3.0 FREE FIELD SOLUTION

The reference solution (for the vessel burst problem) is computed using a 1D point-symmetric Finite Volume approach (the spatial resolution is of 1mm). This solution is then compared with solutions obtained from 2D simulations of Europlexus [10] and 3D simulations with FLACS [11].

The 2D simulation domain in Europlexus is chosen to be 8m long and 6m high. The solution sensitivity to the spatial resolution is investigated using two grids: one with a sell of  $R_{rb}/128=2cm$  and the coarser one of  $R_{rb}/32=8cm$ . The reference solution at  $t = 12ms$  is compared to the one obtained using Europlexus (for 2 different spatial resolutions), see figure 3.

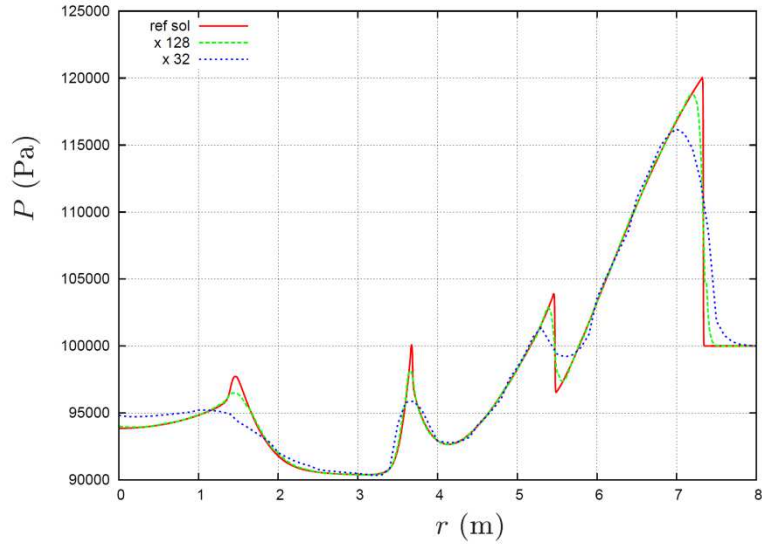


Figure 3: Solution of the reservoir burst problem at  $t = 12$  ms. Europlexus results (for two meshes) versus the reference solution.

A fine mesh is essential for a relatively accurate (with less than 10% error) representation of the overpressure. Moreover, as the distance from the reservoir increases, the relative error on the maximum overpressure also increases. The accuracy of the positive impulse (corresponding to the main pressure peak) is the same order of magnitude at 3.65 m and at 5.6 m.

FLACS is a 3D code also tested for free field pressure propagation. The simulation domain is taken to be 20 m in both horizontal directions and 10m in the vertical direction. The influence of the computational domain size is checked by using a larger domain (30mx30x15m), and the solution is found to be independent on the domain size. The gravity is activated and is parallel to the vertical Z axis. A very short time step is used (CFLC=0.1, CFLV=0.1, also the option “keep low” is activated to prevent time step from growing). The solution is computed with 5 different spatial resolutions, with a mesh size equal to 20 cm, 10 cm, 8 cm, 7 cm and 5 cm. The meshes are regular with constant cell size (see fig 4).

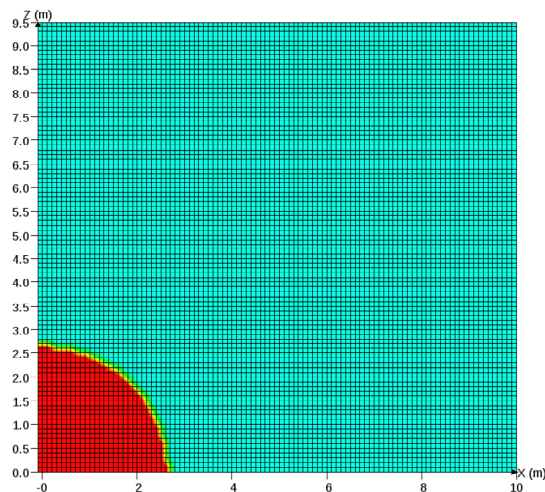


Figure 4. The standard mesh and initial vessel representation using FLACS ( $dx=10$ cm grid size).

The overpressure computed with spatial resolutions of 5cm, 7cm and 8cm shows an error of the same order of magnitude (see fig 5) compared to the reference solution. The positive impulse of the main

pressure peak is closer to the reference solution for the finest resolution (5cm). However the error, even in this case, is greater than 10%. As the distance from the reservoir increases, the error on the positive impulse remains the same.

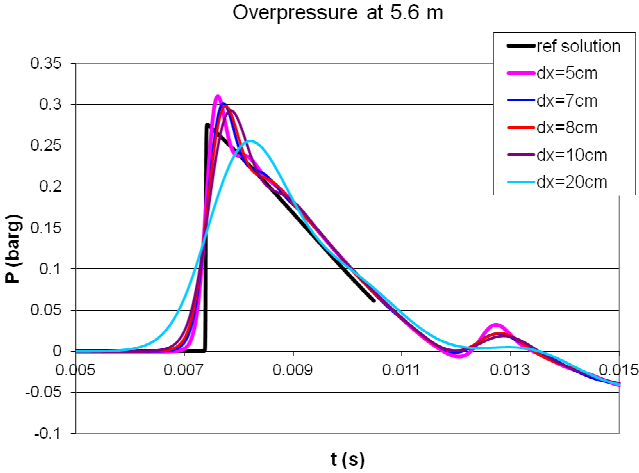


Figure 5. Solution of the reservoir burst problem. Pressure as function of time at R = 5.6 m: FLACS simulation results for various spatial resolutions vs ref solution.

Both softwares FLACS and Europlexus give fair results. Concerning FLACS the main (first) pressure peak and the corresponding positive impulse are slightly overestimated. The best match with the reference solution is obtained for the finest grid (around 10%), however the grid with spatial resolution of 10cm also gives acceptable results.

**4.0 SOLUTION WITH A WALL**

The aim of this section is to investigate numerically the efficiency of protection barriers to mitigate the pressure wave’s propagation. For this purpose the propagation of a pressure wave in a free field is compared to the pressure propagation in the environment with a protective barrier (a wall). The wall is located 9.2m downstream of the centre of the vessel. This position corresponds to an incoming overpressure of ~150 mbarg. The height of the wall is set to 2.5 m, its thickness to 0.5m. In the reference case the wall is considered to have an infinite length (the same size as the computational domain width). Monitoring points are located upstream, downstream and on the wall to study its mitigation effects, see fig 6. Monitoring points located at 1.5m height are of special interest since they correspond to the average height of the lungs of an adult.

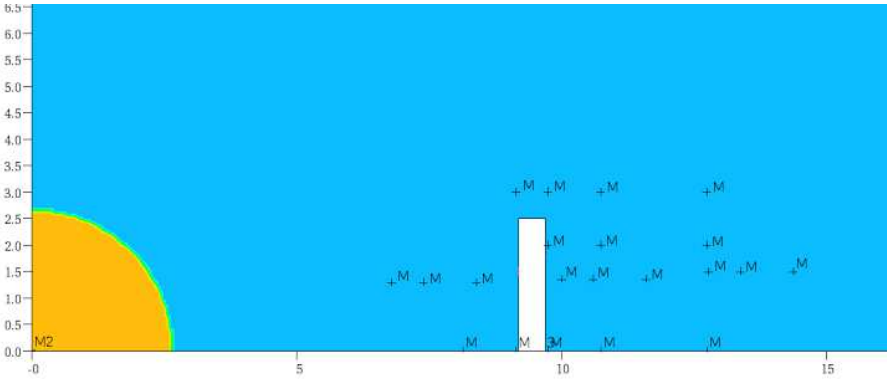


Figure 6. Reservoir burst problem with a wall, monitoring positions.

In order to evaluate the protection barrier efficiency (its mitigation factor) and its dependence on the barrier length, 3D simulations must be validated. For this purpose 3D solution obtained with FLACS

code for reference case is compared to a finer resolved 2D solution from the Eulerian EUROPLEXUS code.

#### 4.1 Numerical settings

In the case of FLACS the grid is the same as in the case of free field. The independence of the numerical solution on the size of the computational domain was verified by comparison of simulation results in three different domains of 90m, 34 m and 26m. However the largest simulation domain is used (in order to reduce the effect of boundary conditions) for the parametric studies considering different lengths of the wall. The sensitivity of simulation results to spatial resolution is verified for two different grids with cell sizes of 5cm and 10cm: simulation results match closely. Hence the solution is independent on grid resolution.

The 2D axisymmetric Euler equations are solved using a Finite Volume approach (see Europlexus' user guide [10]). The height of the computational domain is 10 m. The mesh is not uniform: close to the barrier the mesh size is ten times smaller than far from it. The sensitivity of the simulation results with respect to the mesh size are verified using three different meshes, see table 2. Simulations show that at the points investigated behind the barrier ( $x > 9.7$  m), the difference between the maximum overpressure is more pronounced (10% between coarse and finest grids, 5% between medium and finest grids) in the points with  $z = 3$  m and is not sensibly important close to the soil. The results from the fine mesh are used in the current work. Initial conditions for 2D Europlexus simulations are imposed by projecting on the 2D axial-symmetric mesh the 1D point-symmetric results of the reservoir burst problem just before the interaction with the barrier occurs. In all computations, the predictor-corrector of Van Leer–Hancock (second order in time and quasi-second order in space) is used (space reconstruction is performed on conservative variables and Barth-Jespersen limiter is employed). CFL is equal to 0.5, and the HLLC method is applied to compute the numerical fluxes at the interfaces (see Europlexus' user guide [10] for details).

Table 2: Mesh description used by Europlexus.

Point	Coarsest	Medium	Finest
$x= 9.75\text{m}, z= 3\text{m}$	0.11678	0.12246	0.12762
$x= 10.75 \text{ m}, z= 3\text{m}$	0.0676	0.07323	0.0779
$x= 12.75\text{m}, z= 3\text{m}$	0.03784	0.0413	0.04307
Number of grid points	35 816	139 264	557 638

#### 4.2 Simulation results: cross-comparison between Europlexus and FLACS

Fig 7 shows the comparison of simulations results obtained by Europlexus and FLACS for vessel burst problem with a wall. First two frames correspond to monitoring points located upstream of the wall, whereas other frames correspond to monitoring points located behind the wall. FLACS results are in close agreement with Europlexus simulations.

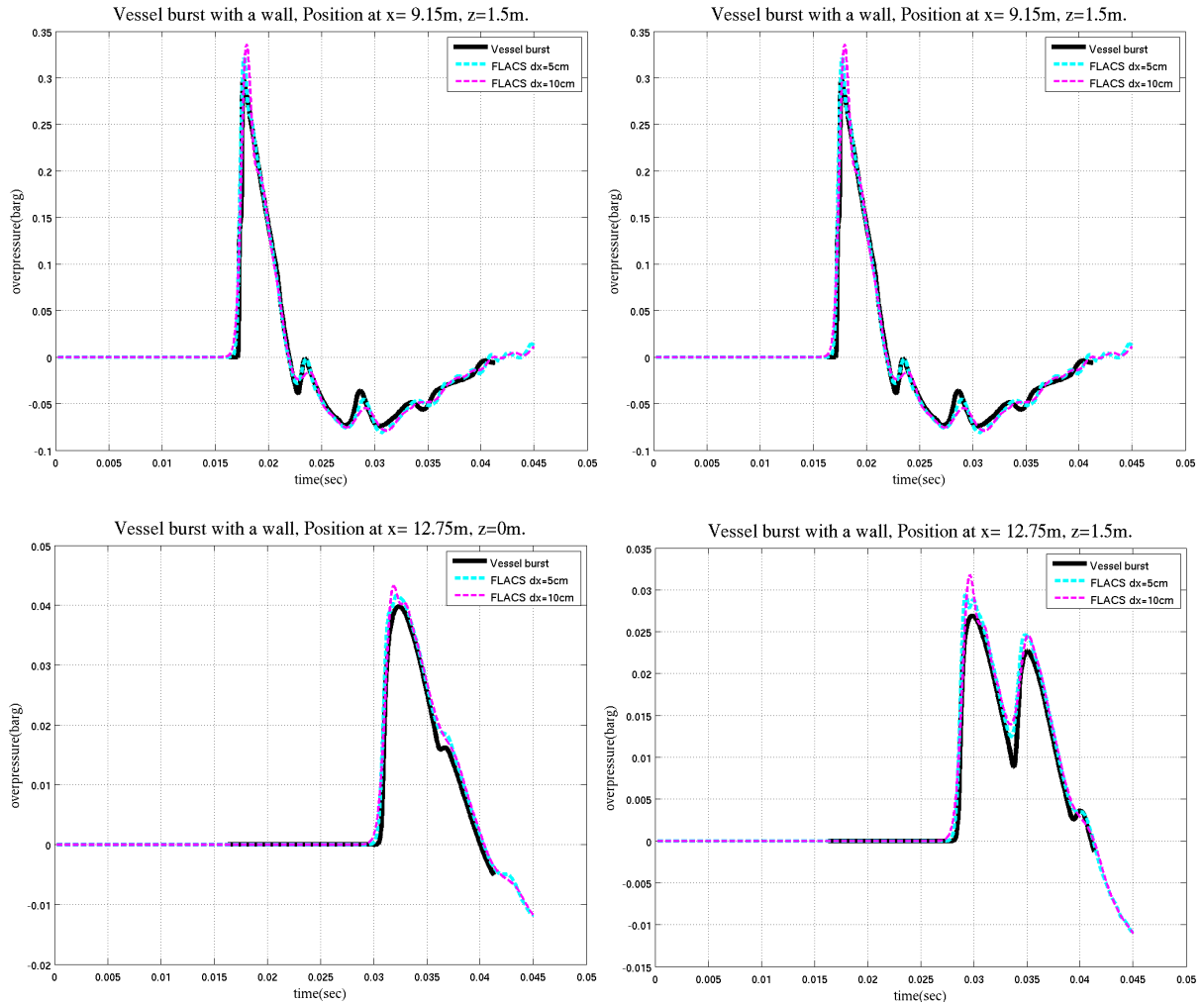


Figure 7. Comparison of Europlexus simulations (in black) to FLACS simulations obtained with different spatial resolutions.

The overpressure computed by FLACS with spatial resolution of  $dx=5$  cm is slightly closer to results of Europlexus in terms of maximum overpressure, time of arrival and corresponding impulse. The solution obtained with FLACS with a spatial resolution of  $dx=10$ cm shows in general a slightly higher pressure than the one computed with a spatial resolution of  $dx=5$  cm. The pressure signal is stiffer for resolution of  $dx=5$  cm, hence pressure curves for  $dx=10$ cm are slightly larger. Thus the impulse computed at the grid with cell size of  $10$ cm is higher. However FLACS simulation results obtained with  $dx=10$ cm are acceptable for further analysis.

In terms of the time corresponding to the detection of the maximum pressure, the error between simulations performed by Europlexus and FLACS (both with  $dx=5$ cm and  $dx=10$ cm) is negligible.

This comparison shows that FLACS results are in very close agreement with Europlexus for the maximum overpressure, for the corresponding impulse and for the time of overpressure arrival.

#### 4.3 Wall effect on the overpressure

To investigate how the presence of wall affects the overpressure propagation upstream and downstream of the wall, one can compare the overpressure maximum in time with and without wall as a function of the distance from the centre of high-temperature and high-pressure reservoir (at  $z=1.5$ m from the ground level), see on fig 8.

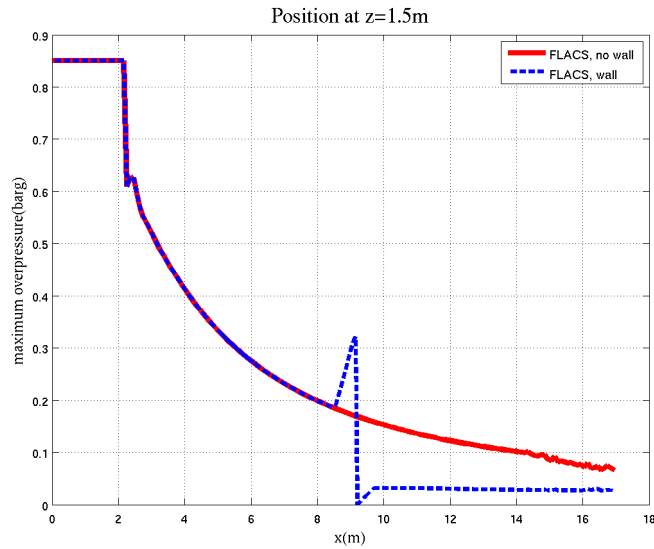


Figure 8. Comparison of FLACS solutions of vessel burst problem with a wall (in blue) and in a free field (in red).

The solutions for the free field and for geometry with a wall (at 9.2m) overlap until 8.5m. Very close to the barrier a significant rise of the overpressure is detected. This is due to the pressure reflection at the wall. Here the reflected overpressure is almost 1.9 times higher than the corresponding free field overpressure, see fig 9.

The first overpressure peak (frame 1, fig 9) corresponds to the overpressure front propagation from the reservoir burst (this peak is identical to the free field solution), whereas the 2<sup>nd</sup> spike on the blue curve (solution with a wall) is the reflected pressure. The closer the monitoring point is located to the wall, the smaller the time gap between these two peaks is and the higher the second spike is. At the monitoring point located 5 cm upstream from the wall, these two peaks add up, leading to the appearance of a single overpressure maximum, which is almost twice higher than the corresponding free field overpressure.

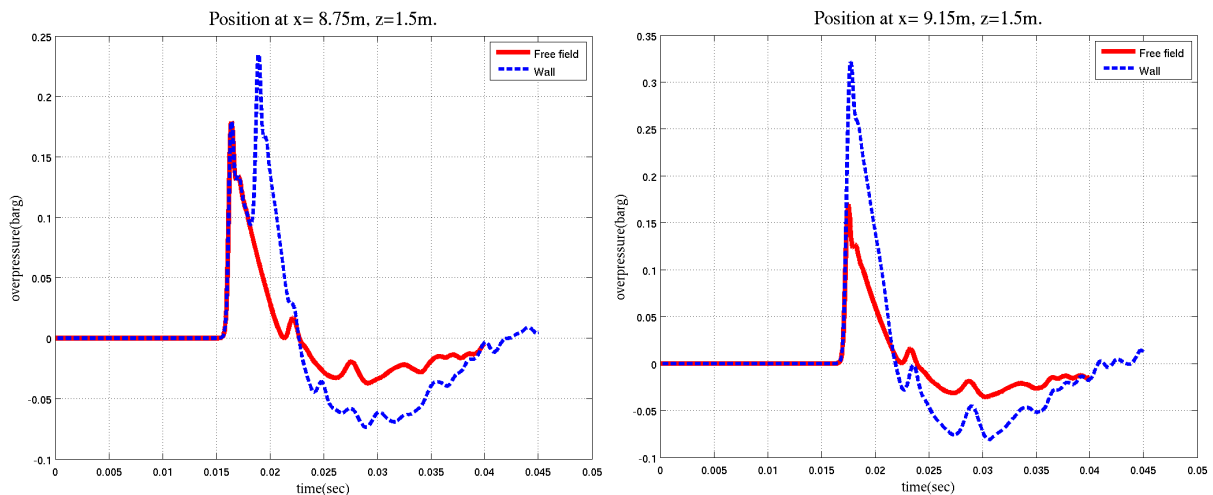


Figure 9. Comparison of FLACS solutions of vessel burst problem with a wall (in blue) and in a free field (in red): upstream of the wall.

Fig. 10 shows the pressure wave propagation downstream of the wall (propagation behind the wall), demonstrating a region of a reduced pressure behind the wall (compared to the free field). This is the so-called “wall shade” effect. The overpressure is significantly reduced compared to the one obtained



for the free field. Figure 10 also demonstrates that behind the barrier (in the reference case) the overpressure does not exceed 32 mbarg at  $z=1.5$  m height from the ground level, which is significantly lower than the overpressure in a free field. The wall not only reduces the pressure wave maximum in its shade, but also leads to the dispersion of the pressure front (reducing the wave front stiffness and increasing its thickness).

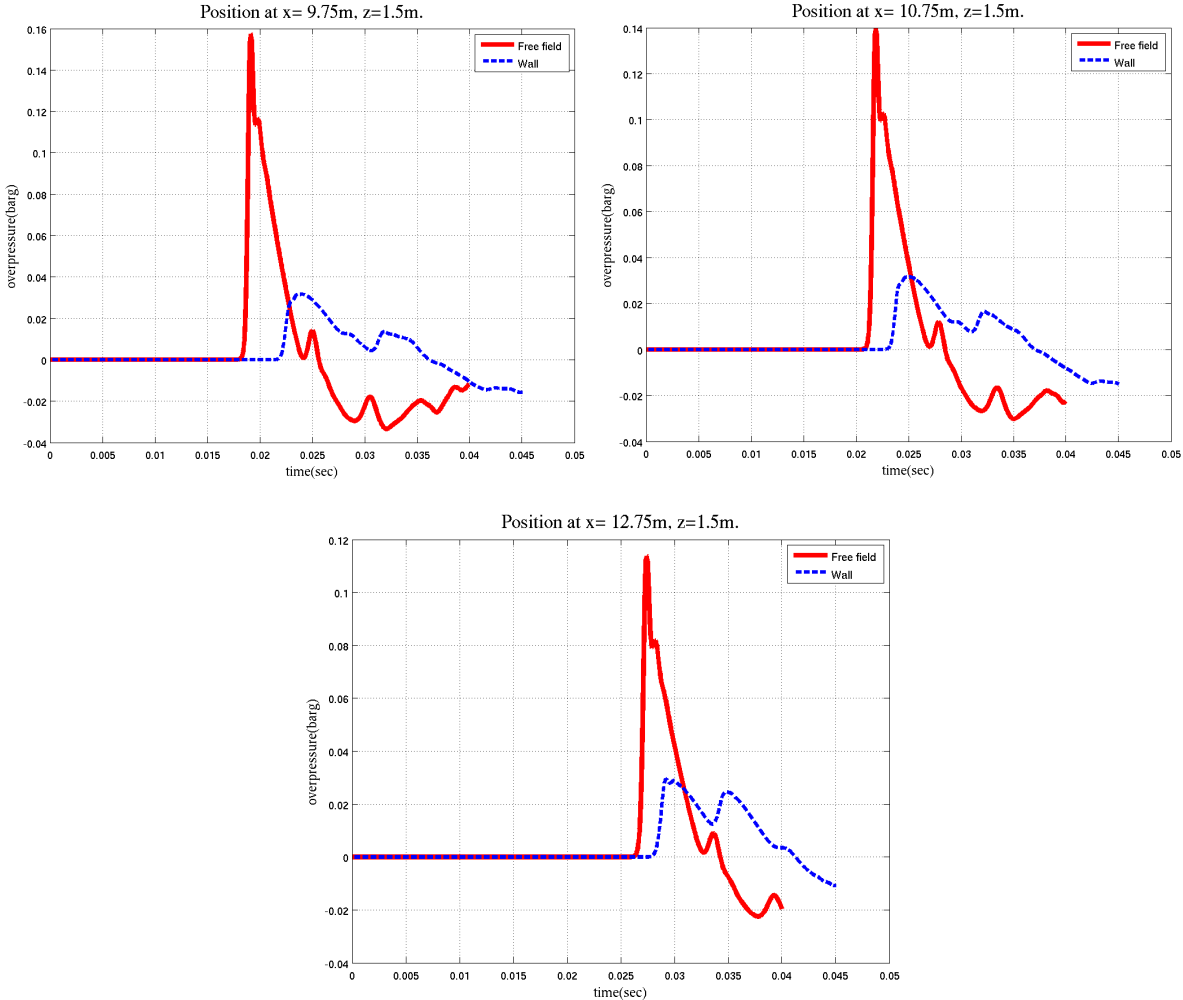


Figure 10. Comparison of pressure signal behind the wall: free field solution is in red, solution with a wall is in blue.

The mitigation factor for the overpressure ( $P_{\max \text{ free field}} / P_{\max \text{ wall}}$ ) demonstrates the efficiency of the protective barrier. Figure 11 shows the pressure mitigation factor versus the downstream distance normalised by the barrier height. This factor shows how many times the free field overpressure is reduced due to the presence of the wall.

At long distances the mitigation factor decreases to 1, meaning that at long distances the pressure in the wall shade approaches the pressure in the free field. Unfortunately, in order to catch this phenomenon one should use a much longer simulation domain. However this becomes very expensive in terms of CPU time.

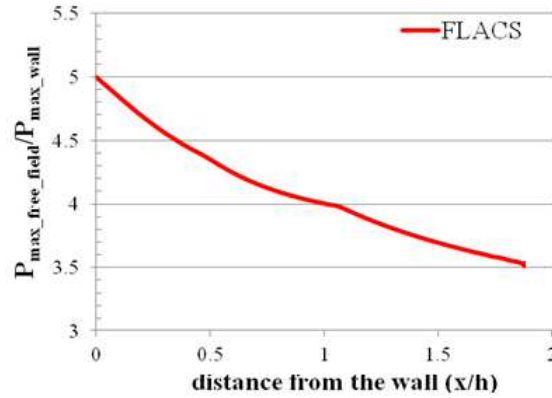


Figure 11. Mitigation factor for the overpressure vs. downstream distance.

#### 4.4 Effect of the wall length on the wall mitigation

An important parameter strongly affecting mitigation of a barrier is its length. The barrier length can significantly reduce its migration properties. For the comparison with the infinite barrier, three finite length walls are considered.

Table 3. Various wall lengths considered.

Wall length L(m)	Ratio L/h
7.8	3.12
15.6	6.24
31.2	12.48
infinite	infinite

The mitigation effect of these walls on the overpressure in the wall shade is shown in figure 12.

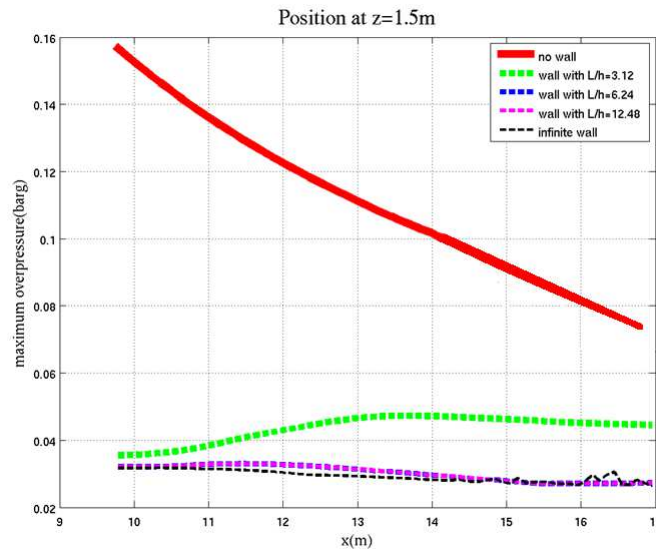


Figure 12. Comparison of maximum overpressure (in the shade, at  $z=1.5\text{m}$  from the ground) for walls with various lengths

In figure 12, the blue curve overlaps the magenta curve. This means that for walls with aspect ratio larger than 6 ( $L/h > 6$ ), the mitigation factors are approximately the same and they approach the mitigation factor of the infinite wall (black curve). For shorter walls, see here for instance  $L/h \sim 3$ , the

mitigation effect is strongly reduced. The overpressure for short walls is much higher than for the infinite wall, due to the pressure wave lateral overturning.

## 5.0 CONCLUSION

The comparison of results from FLACS 3D simulations to 2D Europlexus simulations shows good agreement for the free field solution and the solution with a wall. This demonstrates FLACS capacities to be used for simulations of pressure wave propagation in the far field for both geometries: free field and for geometry with a wall.

Parametrical simulations performed by FLACS showed that for short walls with aspect ratio ( $L/h < 6$ ) the mitigation factor for the overpressure ( $P_{\max \text{ free field}} / P_{\max \text{ wall}}$ ) is significantly reduced compared to the infinite wall, due to the appearance of the lateral overturning waves. Hence it is recommended to build a wall along the whole perimeter of the protected zone to avoid overturning.

## 6.0 REFERENCES

1. NOTA recommandations 2009 version française - Guide SFEPA No.9, 2009, Guide des Bonnes Pratiques en Pyrotechnie.
2. Allain, L., Barricade influence on blast wave propagation, SNPE / Division Défense Espace Report, 1994.
3. Borgers, J., Blast walls reviewed, 21<sup>st</sup> Military Aspects of Blast and Shock Conference, October 4 – 8th 2010, Jerusalem (Israel), 2010.
4. Jallais, S., Effectiveness of protective barriers against H<sub>2</sub> hazards: Literature survey, R&D CRCO Internal Report No. GPE/2009/97.
5. Sedov, L.I., Similarity and Dimensional Methods in Mechanics, 1959, Academic Press, New York.
6. Kuhl, A.L., Kamel, M.M., Oppenheim, A.K., Pressure Waves Generated by Steady Flames, 14<sup>th</sup> Symposium (International) on Combustion, The Combustion Institute, Pittsburgh, Pennsylvania, pp. 1201-1215, 1973.
7. Beccantini, A., Malczynskil, A., and Studer, E., Comparison of TNT-equivalence approach, TNO multi-energy approach and a CFD approach in investigating hemispheric hydrogen-air vapour cloud explosions. Proc. of 5<sup>th</sup> International Seminar on Fire and Explosion Hazards, April 2007, Edinburgh.
8. Garcia, J., Baraldi, D., Gallego, E., Beccantini, A., Crespo, A., Hansen, O.R., Hoiset S., Kotchourko, A., Makarov, D., Migoya, E., Molkov, V., Voort, M.M., Yanez, J., An intercomparison exercise on the capabilities of CFD models to reproduce a large-scale hydrogen deflagration in open atmosphere, *International Journal of Hydrogen Energy*, **35**, 2010, pp. 4435–4444.
9. Beccantini, A., Vyazmina, E., Trélat S., Reference solutions for CFD code validation in computing the mitigation effect of a barrier in case of Vapor Cloud Explosions, deliverable report of ANR BARPPRO, 2013.
10. EUROPLEXUS Users Manual, on-line version: <http://europlexus.jrc.ec.europa.eu>.
11. FLACS overview: [http://gexconus.com/FLACS\\_overview](http://gexconus.com/FLACS_overview).